Electronic Supplementary Material (ESI) for Catalysis Science & Technology

Palladium Catalytic Systems with Hybrid Pyrazole Ligands in C-C Coupling Reactions. Nanoparticles *versus* Molecular Complexes

Daniel Peral[a], Fernando Gómez-Villarraga[a], Xavier Sala[a], Josefina Pons[a], J. Carles Bayón[a], Josep Ros[a], Miguel Guerrero[b,c], Laure Vendier[b,c], Pierre Lecante[d], Jordi García-Antón*[a], and Karine Philippot*[b,c]

[a] D. Peral, F. Gómez-Villarraga, Dr. J. García-Antón, Dr. X. Sala, Dr. J. Pons, Prof. J.C. Bayón, Prof. J. Ros
Departament de Química, Unitat de Química Inorgànica, Universitat Autònoma de Barcelona, 08193-Bellaterra, Barcelona, Spain.
Fax: (+34) 93 581 3101
*E-mail: Jordi.GarciaAnton@uab.es

[b] Dr. M. Guerrero, Dr. L. Vendier, Dr. K. Philippot
CNRS; LCC (Laboratoire de Chimie de Coordination du CNRS), 205, route de Narbonne, F-31077 Toulouse, France
Fax: (+33) 5 61553003
*E-mail: Karine.Philippot@lcc-toulouse.fr

[c] Université de Toulouse; UPS, INPT; LCC; F-31077 Toulouse, France

[d] CNRS, CEMES (Centre d'Elaboration de Matériaux et d'Etudes Structurales), 29 rue J. Marvig, F-31055 Toulouse, France

Supplementary information

Supplementary Information

Tables:

Figures:

Figure S7. DLS measurement for **N4** (Diameter = 79 nm).

Figure S8. Transferred NOESY NMR spectrum for **N3**.

Figure S9. ORTEP drawing of the two non-equivalent molecules of $[PdCl_2(L1)_2]$ (**C1**)

Figure S10. ORTEP drawing of the two non-equivalent molecules of $[PdCl_2(L2)]$ (**C2**)

Figure S11. ORTEP drawing of the two non-equivalent molecules of $[PdCl_2(L3)]$ (**C3**)

Figure S12. DOSY NMR for the "[Pd(0)(dba) $(L1)_2$]" complex

Figure S13. DOSY NMR spectrum for the "[Pd(0)(dba)(L3)]" complex

Discussion:

Discussion S1. NMR Studies of C1-C4

Table S1. Selected bond lengths (Å) and bond angles (deg) for **C1-C4** complexes.

C1 (molecule A)		**C1 (molecule B)**	
Pd(1) – N(1)	2.036(9)	Pd(2) – N(5)	2.031(8)
Pd(1) – N(3)	2.019(8)	Pd(2) – N(7)	1.991(8)
Pd(1) – Cl(1)	2.300(3)	Pd(2) – Cl(3)	2.294(3)
Pd(1) – Cl(2)	2.304(3)	Pd(2) – Cl(4)	2.313(3)
N(1) – Pd(1) – N(3)	174.9(4)	N(5) – Pd(2) – N(7)	174.8(4)
N(1) – Pd(1)– Cl(1)	91.8(2)	N(5) – Pd(2)– Cl(3)	90.0(2)
N(3) – Pd(1) – Cl(1)	89.7(3)	N(7) – Pd(2) – Cl(3)	88.1(2)
N(1) – Pd(1)– Cl(2)	90.3(2)	N(5) – Pd(2)– Cl(4)	92.3(2)
N(3) – Pd(1) – Cl(2)	88.5(3)	N(7) – Pd(2) – Cl(4)	89.9(2)
Cl(1) – Pd(1)– Cl(2)	176.38(12)	Cl(3) – Pd(2)– Cl(4)	176.17(12)
C2 (molecule A)		**C2 (molecule B)**	
Pd(1) – N(1)	2.0305(17)	Pd(2) – N(3)	2.0236(17)
Pd(1) – S(1)	2.2792(6)	Pd(2) – S(2)	2.2822(6)
Pd(1) – Cl(1)	2.2934(6)	Pd(2) – Cl(3)	2.2892(6)
Pd(1) – Cl(2)	2.3180(6)	Pd(2) – Cl(4)	2.3176(6)
N(1) – Pd(1) – S(1)	91.71(5)	N(3) – Pd(2) – S(2)	91.55(5)
N(1) – Pd(1)– Cl(1)	177.63(5)	N(3) – Pd(2)– Cl(3)	177.94(5)
S(1) – Pd(1) – Cl(1)	86.01(2)	S(2) – Pd(2) – Cl(3)	86.39(2)
N(1) – Pd(1)– Cl(2)	90.54(5)	N(3) – Pd(2)– Cl(4)	90.33(5)
S(1) – Pd(1) – Cl(2)	174.62(2)	S(2) – Pd(2) – Cl(4)	174.64(2)
Cl(1) – Pd(1)– Cl(2)	91.68(2)	Cl(3) – Pd(2)– Cl(4)	91.71(2)
C3 (molecule A)		**C3 (molecule B)**	
Pd(1) – N(1)	2.0214(13)	Pd(2) – N(4)	2.0100(13)
Pd(1) – N(3)	2.0505(13)	Pd(2) – N(6)	2.0628(12)
Pd(1) – Cl(1)	2.2901(4)	Pd(2) – Cl(3)	2.3109(4)
Pd(1) – Cl(2)	2.3002(4)	Pd(2) – Cl(4)	2.2884(4)
N(1) – Pd(1) – N(3)	89.24(5)	N(4) – Pd(2) – N(6)	90.16(5)
N(1) – Pd(1)– Cl(1)	176.62(4)	N(6) – Pd(2) – Cl(3)	173.03(4)
N(3) – Pd(1) – Cl(1)	87.39(4)	N(4) – Pd(2)– Cl(3)	89.93(4)
N(1) – Pd(1)– Cl(2)	92.03(4)	N(6) – Pd(2) – Cl(4)	88.13(4)
N(3) – Pd(1) – Cl(2)	177.89(4)	N(4) – Pd(2)– Cl(4)	178.05(4)
Cl(1) – Pd(1)– Cl(2)	91.349(17)	Cl(3) – Pd(2)– Cl(4)	91.879(17)
C4			
Pd(1) – N(1)	2.0382(11)	Pd(1) – Cl(1)	2.2942(3)
Pd(1) – N(3)	2.1241(10)	Pd(1) – Cl(2)	2.2987(3)
N(1) – Pd(1) – N(3)	91.41(4)	N(1) – Pd(1) – Cl(2)	174.12(3)
N(1) – Pd(1)– Cl(1)	89.22(3)	N(3) – Pd(1)– Cl(2)	91.79(3)
N(3) – Pd(1) – Cl(1)	173.10(3)	Cl(1) – Pd(1) – Cl(2)	88.186(14)

Table S2. Optimization of the Suzuki-Miyaura conditions for molecular complexes.

[substrate] / [Pd]	Solvents (10 mL)	Base	Conversion (%)	Chemoselectivity (%)	Yield 4-Methylbiphenyl (%)	TON
500	DMF (10)	^{t}BuOK	2	0	0	0
500	DMF (10)	NEt_3	0	0	0	0
500	Toluene (10)	^{t}BuOK	0	0	0	0
500	Toluene (10)	NEt_3	< 1	100	< 1	< 5
500	Toluene:H_2O (8:2)	^{t}BuOK	3	100	3	15
500	Dioxane:H_2O (8:2)	^{t}BuOK	49	100	49	245
500	DMF:H_2O (9.5:0.5)	^{t}BuOK	49	87	42	210
500	DMF:H_2O (9.5:0.5)	NEt_3	13	92	12	60
500	DMF:H_2O (8:2)	NEt_3	25	100	25	125
500	DMF:H_2O (8:2)	Na_2CO_3	71	86	61	310
500	DMF:H_2O (8:2)	K_2CO_3	77	81	62	312
500	DMF:H_2O (8:2)	^{t}BuOK	78	94	73	365
2500	**DMF:H_2O (8:2)**	**^{t}BuOK**	**25**	**93**	**23**	**575**
5000	DMF:H_2O (8:2)	^{t}BuOK	9	90	8	400

Conditions: 2.5 mmol 4-bromotoluene, 3.1 mmol phenylboronic acid, 5.0 mmol of base, 0.5 mmol naphthalene as internal standard, 100ºC, 6 h, 1200 rpm. All tests were performed using the appropriate amount of **C4** as catalyst.

Table S3. Complete data for the Suzuki-Miyaura reactions with Pd complexes.

Pd complex	L/Pd	X	Conversion (%)	Chemoselectivity (%)
$[PdCl_2(CH_3CN)_2]$	-	Br	30	82
		I	100	58
$[Pd_2(dba)_3]$	-	Br	39	95
		I	100	49
$[PdCl_2(CH_3CN)_2]$	**L1** (1:1)	Br	25	93
		I	55	90
	L1 (1:2)	Br	29	88
		I	63	61
C1	-	Br	19	94
		I	43	61
$[Pd_2(dba)_3]$	**L1** (1:1)	Br	16	83
		I	56	87
	L1 (1:2)	Br	25	86
		I	64	66
$[PdCl_2(CH_3CN)_2]$	**L2** (1:1)	Br	27	79
		I	51	56
	L2 (1:2)	Br	31	84
		I	47	69
C2	-	Br	26	84
		I	85	57
$[Pd_2(dba)_3]$	**L2** (1:1)	Br	12	57
		I	59	67
	L2 (1:2)	Br	25	81
		I	58	63
$[PdCl_2(CH_3CN)_2]$	**L3** (1:1)	Br	26	80
		I	64	88
	L3 (1:2)	Br	32	85
		I	59	74
C3	-	Br	52	91
		I	74	58
$[Pd_2(dba)_3]$	**L3** (1:1)	Br	23	72
		I	64	66
	L3 (1:2)	Br	34	70
		I	46	82
$[PdCl_2(CH_3CN)_2]$	**L4** (1:1)	Br	28	79
		I	56	86
	L4 (1:2)	Br	35	90
		I	55	50
C4	-	Br	25	93
		I	48	70
$[Pd_2(dba)_3]$	**L4** (1:1)	Br	16	82
		I	59	81
	L4 (1:2)	Br	9	83
		I	40	81

Conditions: $1 \cdot 10^{-3}$ mmol $[Pd(Cl)_2(CH_3CN)_2]$ or $[Pd_2(dba)_3]$, 2.5 mmol 4-bromotoluene or 4-iodotoluene, 3.1 mmol phenylboronic acid, 5.0 mmol ^tBuOK, 0.5 mmol naphthalene as internal standard, 8.0 ml DMF, 2.0 ml H_2O, 100ºC, 6 h, 1200 rpm.

Table S4. Complete data for the homocoupling catalytic reactions with Pd NPs.

NP	Substrate	Conversion (%)	Chemoselectivity homocoupling (%)	Chemoselectivity Toluene (%)
Pd/C	Cl-Tol	2	0	100
	Br	83	41	59
	I	100	1	99
N1	Cl-Tol	1	0	100
	Br	17	11	89
	I	11	0	100
N2	Cl-Tol	1	0	100
	Br	18	24	76
	I	100	0	100
N3	Cl-Tol	< 1	0	100
	Br	64	70	30
	I	100	0	100
N4	Cl-Tol	< 1	0	100
	Br	10	5	95
	I	9	0	100

Conditions: $1 \cdot 10^{-2}$ mmol Pd atoms, 2.5 mmol 4-halogenotoluene (Cl-Tol, Br or I), 5.0 mmol ^{t}BuOK, 0.5 mmol naphthalene as internal standard, 8.0 ml DMF, 2.0 ml H_2O, 100ºC, 6 h, 1200 rpm.

Table S5. Crystallographic data for **C1-C4** complexes.

	C1	**C2**	**C3**	**C4**
Molecular Formula	$C_{30}H_{56}Cl_2N_4O_2Pd$	$C_{15}H_{28}Cl_2N_2PdS$	$C_{15}H_{29}Cl_2N_3Pd$	$C_{23}H_{45}Cl_2N_3Pd$
Formula weigh	682.09	445.75	428.71	540.92
Temperature (K)	180(2)	180(2)	180(2)	180(2)
Wavelength (Å)	0.71073	0.71073	0.71073	0.71073
System, space group	Triclinic, P1	Triclinic, P-1	Triclinic, P-1	Monoclinic, $P2_1/c$
Unit cell dimensions				
a (Å)	8.1693(8)	8.1752(8)	8.1051(8)	15.7877(10)
b (Å)	9.1162(10)	15.2655(6)	11.1155(9)	21.0937(13)
c (Å)	22.9935(7)	15.4570(10)	22.6264(6)	8.1090(5)
α (º)	93.592(3)	94.321(7)	77.784(5)	90
β (º)	91.806(5)	90.451(5)	89.987(4)	102.061(3)
γ (º)	89.939(6)	93.185(4)	71.894(3)	90
U ($Å^3$)	1708.2(3)	1920.4(2)	1888.9(2)	2640.9(3)
Z	2	4	4	4
D_{calc} (g cm^{-3})	1.326	1.542	1.508	1.360
μ (mm^{-1})	0.731	1.349	1.263	0.919
F(000)	720	912	880	1136
Crystal size (mm^3)	0.17x0.08x0.02	0.18x0.1x0.02	0.2x0.12x0.04	0.22x0.12x0.03
hkl ranges	-9≤h≤9, -10≤k≤10, -27≤l≤27	-10≤h≤10, -19≤k≤12, -19≤l≤19	-10≤h≤10, -13≤k≤13, -28≤l≤27	-25≤h≤26, -34≤k≤35, -13≤l≤13
2 θ Range (º)	3.35 to 25.35	1.32 to 26.37	1.98 to 26.37	1.93 to 36.96
Reflections collected/unique/ [R_{int}]	19788/11748 [R(int) = 0.0838]	30197/7799 [R(int) = 0.0203]	41896/7685 [R(int) = 0.0177]	124677/13366 [R(int) = 0.0350]
Completeness to θ (θ = 25.00º)	99.7%	99.4%	99.5%	99.8%
Absorption correction	Semi-empirical	Semi-empirical	Semi-empirical	Semi-empirical
Data/restrains/parameters	11748/3/686	7799/0/385	7685/0/385	13366/0/266
Goodness-of-fit on F^2	1.016	1.057	1.085	1.074
Final R indices [I>2 σ (I)]	R1 = 0.0759, wR_2 = 0.1632	R1 = 0.0225, wR_2 = 0.0548	R1 = 0.0161, wR_2 = 0.0393	R1 = 0.0311, wR_2 = 0.0593
R indices (all data)	R1 = 0.1022, wR_2 = 0.1820	R1 = 0.0272, wR_2 = 0.0585	R1 = 0.0182, wR_2 = 0.0409	R1 = 0.0553, wR_2 = 0.0682
Largest diff. peak and hole (e $Å^{-3}$)	3.986 and -1.075	0.776 and -0.581	0.323 and -0.461	0.781 and -0.612

Figure S1. HR-TEM micrographs and the corresponding size- histograms of Pd nanoparticles synthesized as following: a) [**L1**]/[Pd]=0.5; b) [**L1**]/[Pd]=1.0; c) [**L1**]/[Pd]=2.0

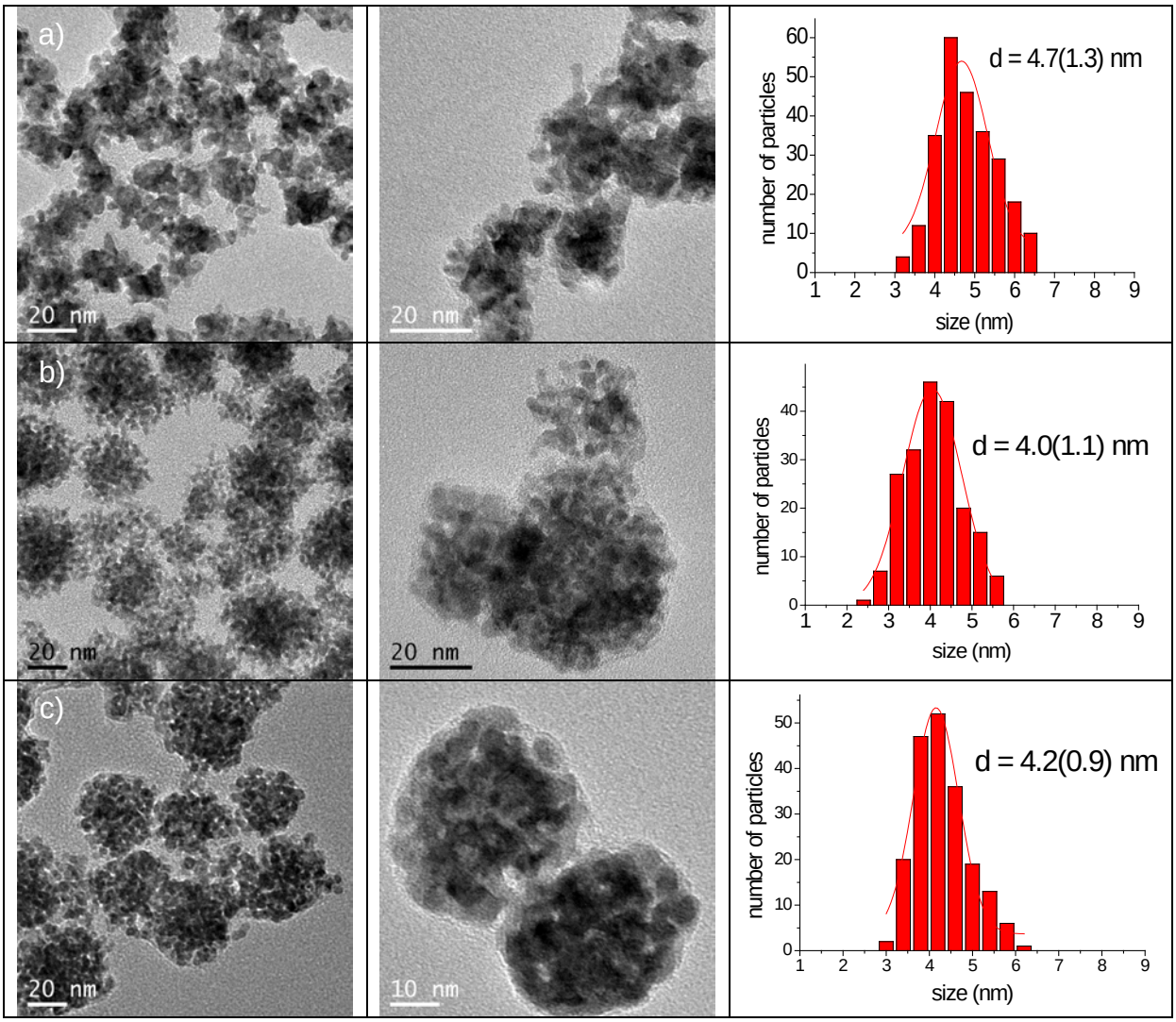

Figure S2. HR-TEM micrographs and the corresponding size- histograms of Pd nanoparticles synthesized as following: a) [**L2**]/[Pd]=0.5; b) [**L2**]/[Pd]=1.0; c) [**L2**]/[Pd]=2.0

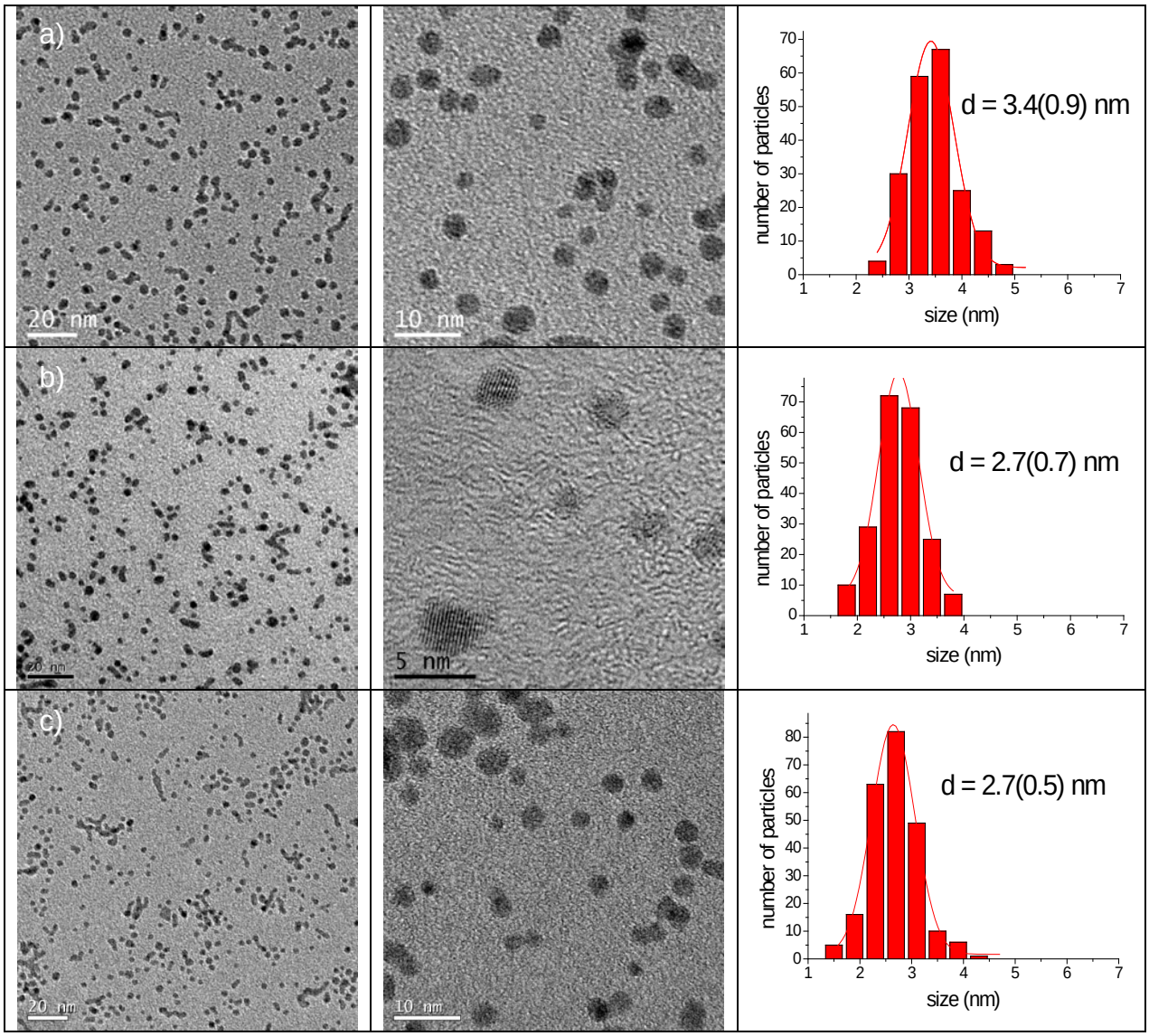

Figure S3. HR-TEM micrographs and the corresponding size- histograms of Pd nanoparticles synthesized as following: a) [**L3**]/[Pd]=0.5; b) [**L3**]/[Pd]=1.0; c) [**L3**]/[Pd]=2.0

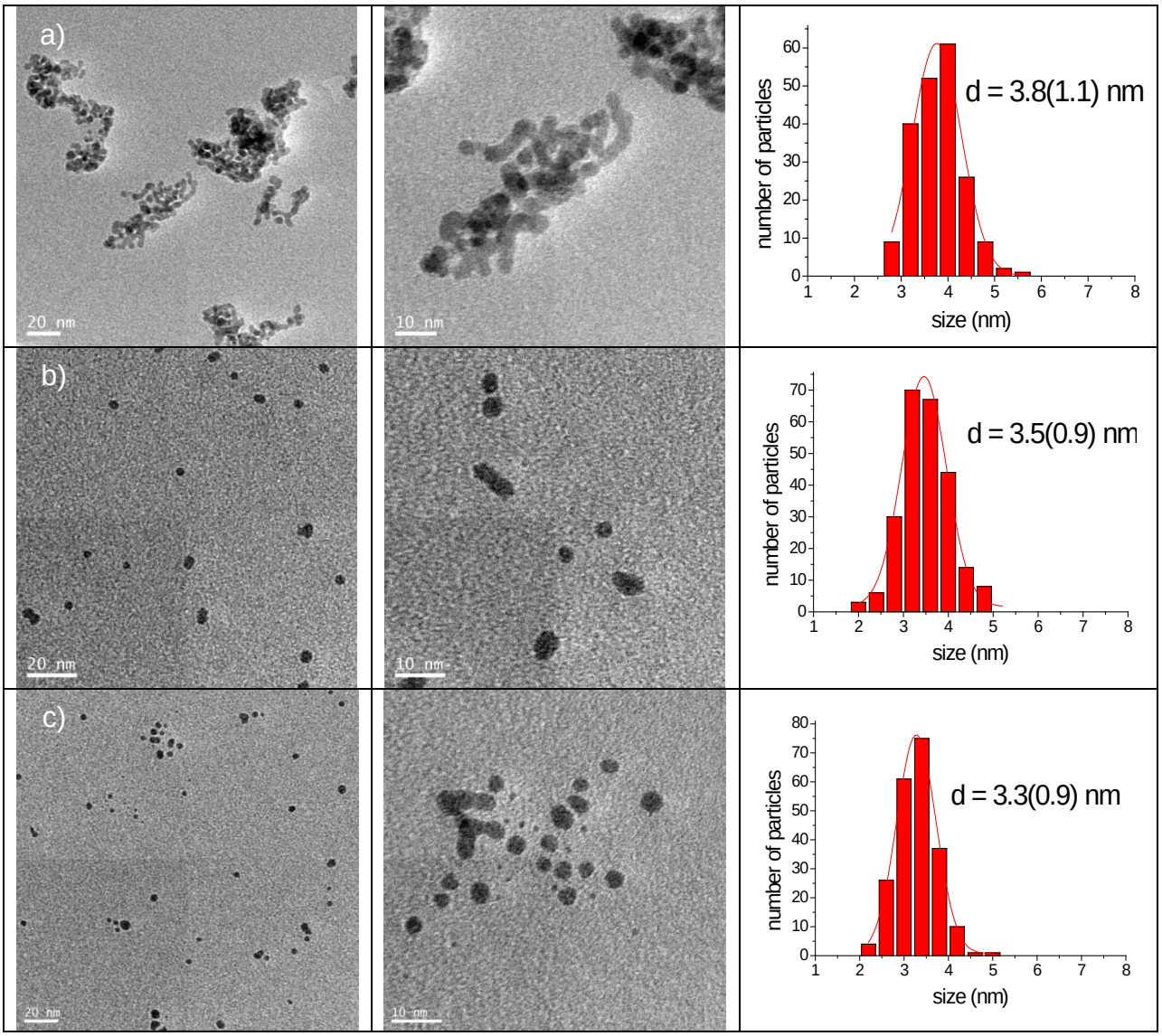

Figure S4. HR-TEM micrographs and the corresponding size- histograms of Pd nanoparticles synthesized as following: a) [**L4**]/[Pd]=0.5; b) [**L4**]/[Pd]=1.0; c) [**L4**]/[Pd]=2.0

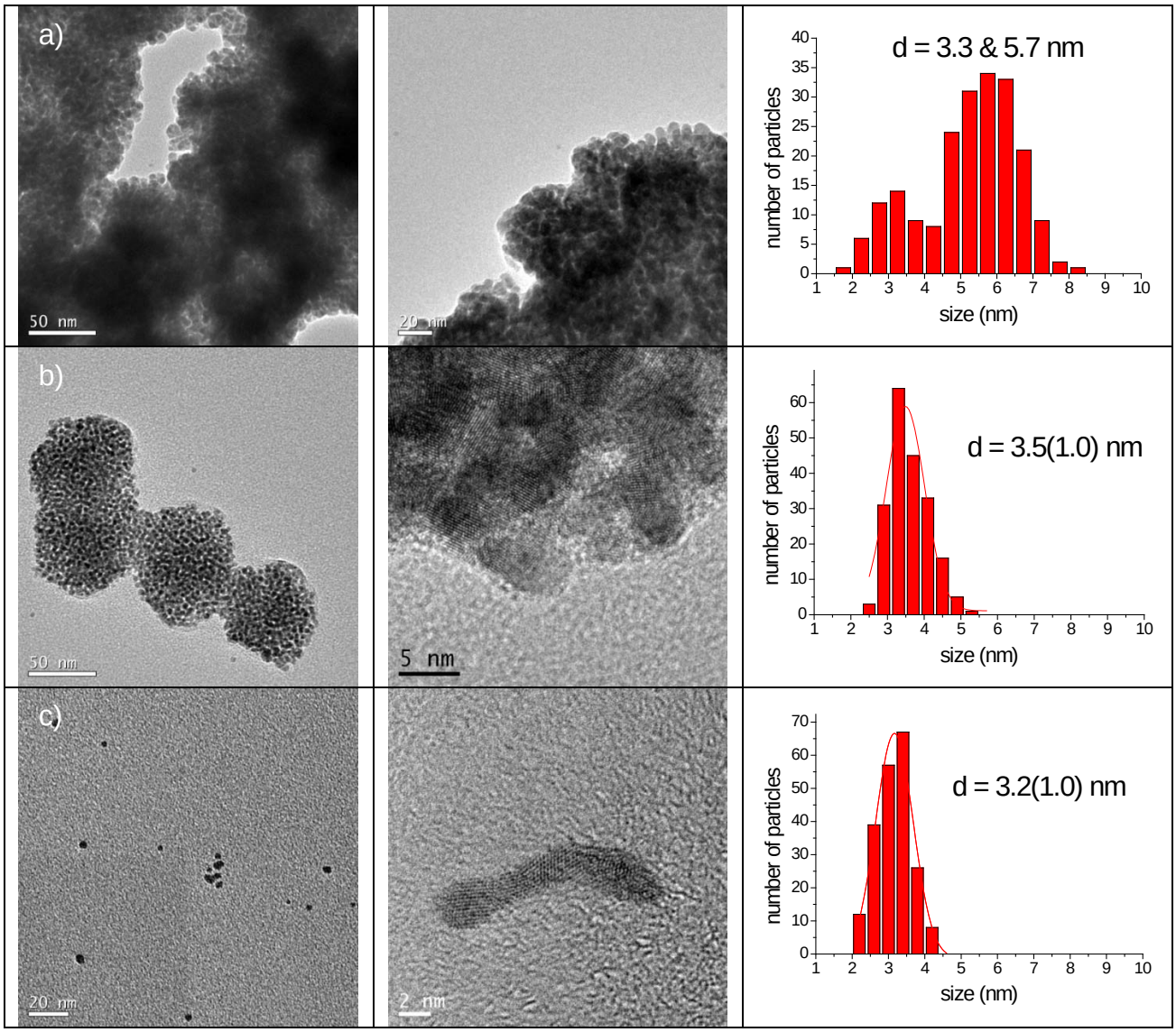

Figure S5. WAXS measurements on Pd nanoparticles for **N1**-**N4** and comparison with Pd fcc in reciprocal space (a) and real space (b).

a)

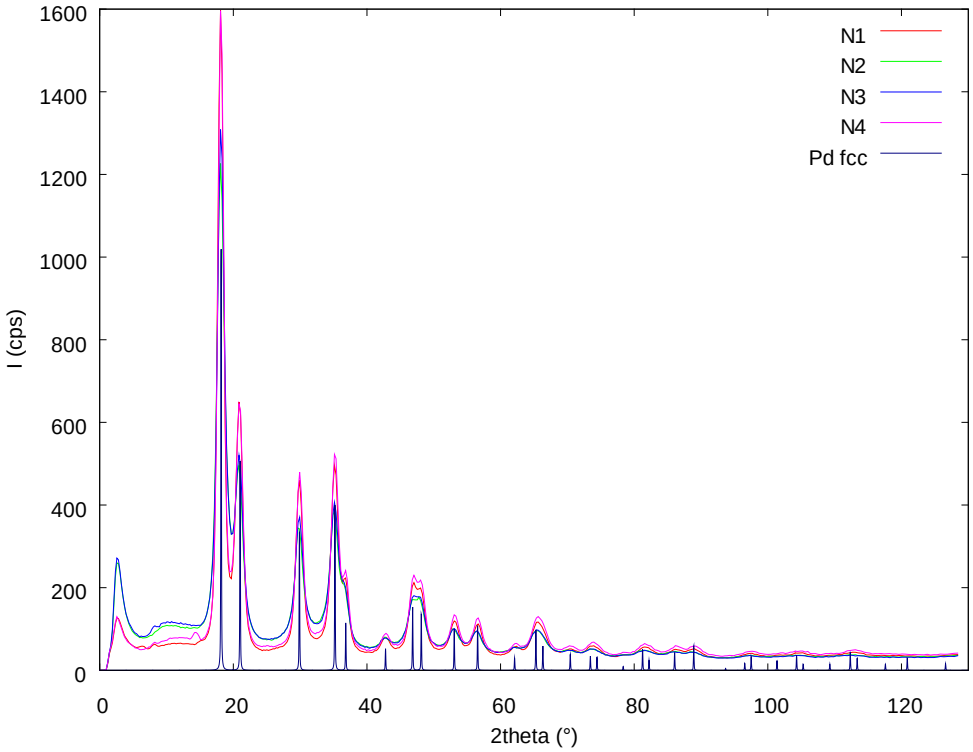

b)

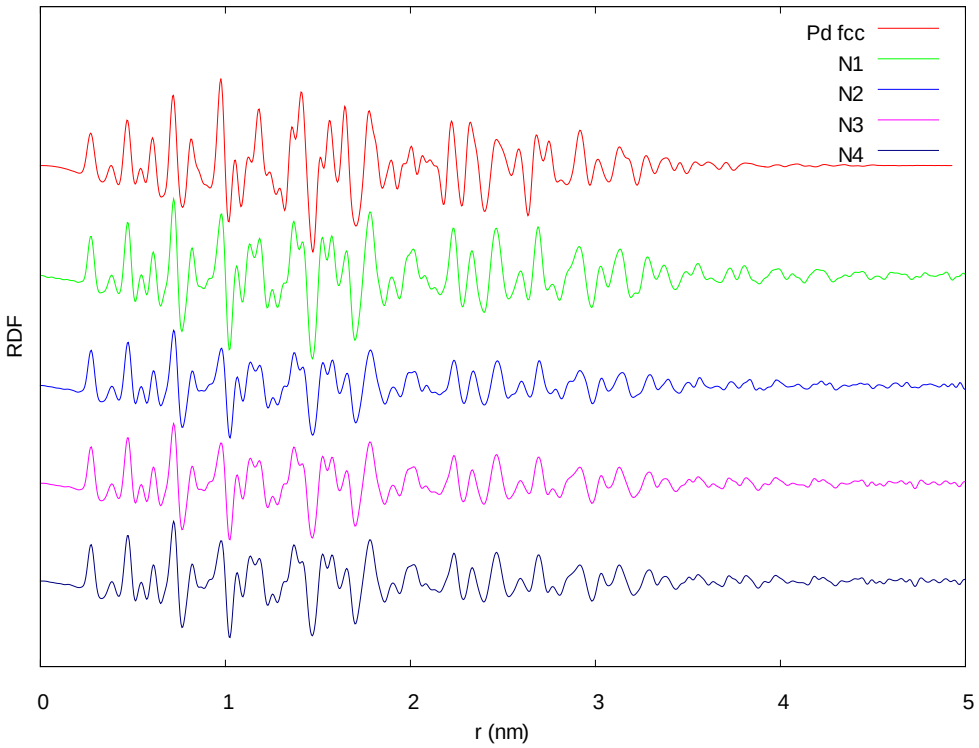

Figure S6. SEM-FEG analyses of the Pd materials produced with a) [**L1**]/[Pd]=0.5; b) [**L1**]/[Pd]=1.0; c) [**L1**]/[Pd]=2.0 and d) [**L4**]/[Pd]=1.0.

A)

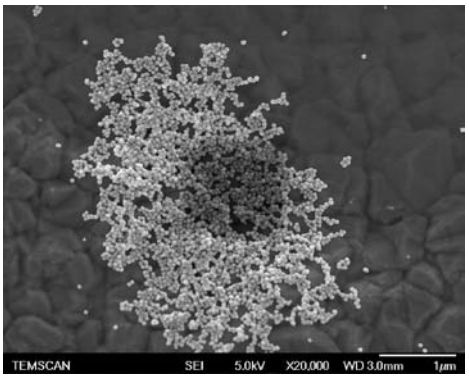

B)

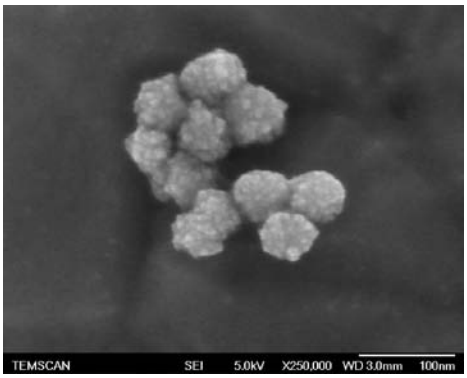

C)

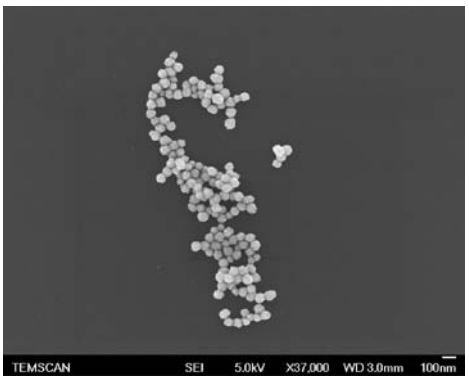

D)

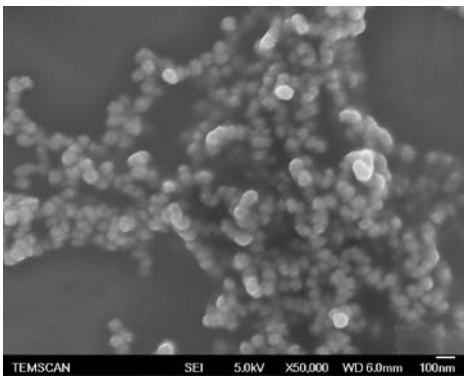

Figure S7. DLS measurement for **N4** (Diameter = 79 nm)

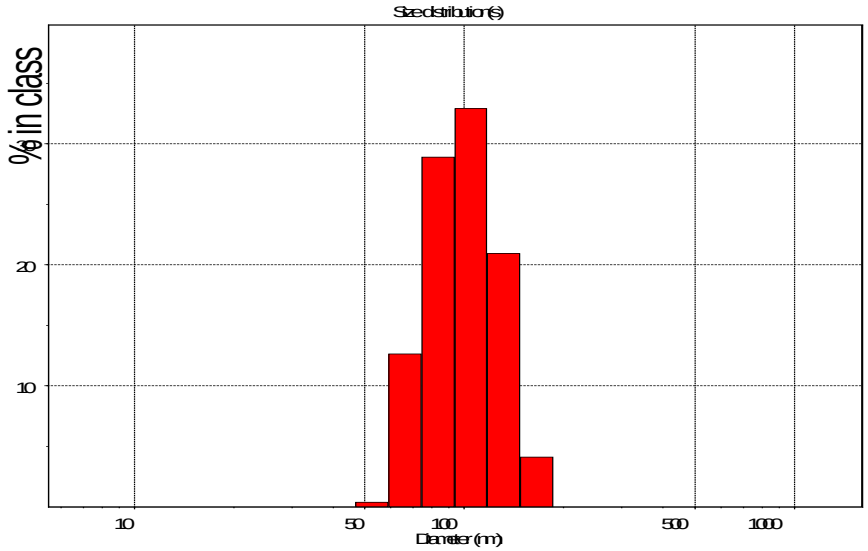

Size(nm)	Intensity	Volume	Number
6.6	0.0	0.0	0.0
8.4	0.0	0.0	0.0
10.5	0.0	0.0	0.0
13.2	0.0	0.0	0.0
16.7	0.0	0.0	0.0
21.0	0.0	0.0	0.0
26.4	0.0	0.0	0.0
33.3	0.0	0.0	0.0
41.9	0.0	0.0	0.1
52.7	0.4	7.7	15.9
66.4	12.7	20.5	36.8
83.6	28.9	23.5	29.2
105.3	32.9	17.6	11.3
132.6	20.9	13.6	4.2
166.9	4.1	11.8	1.7
210.1	0.0	5.2	0.7
264.6	0.0	0.0	0.0
333.1	0.0	0.0	0.0
419.4	0.0	0.0	0.0
528.1	0.0	0.0	0.0
664.9	0.0	0.0	0.0
837.1	0.0	0.0	0.0
1054.0	0.0	0.0	0.0
1327.0	0.0	0.0	0.0

Peak Analysis by intensity			
Peak	Area	Mean	Width
1	100.0	102.1	71.2

Peak Analysis by volume			
Peak	Area	Mean	Width
1	100.0	104.6	110.4

Peak Analysis by number			
Peak	Area	Mean	Width
1	100.0	79.1	42.3

Figure S8. Transferred NOESY NMR spectrum for **N3**.

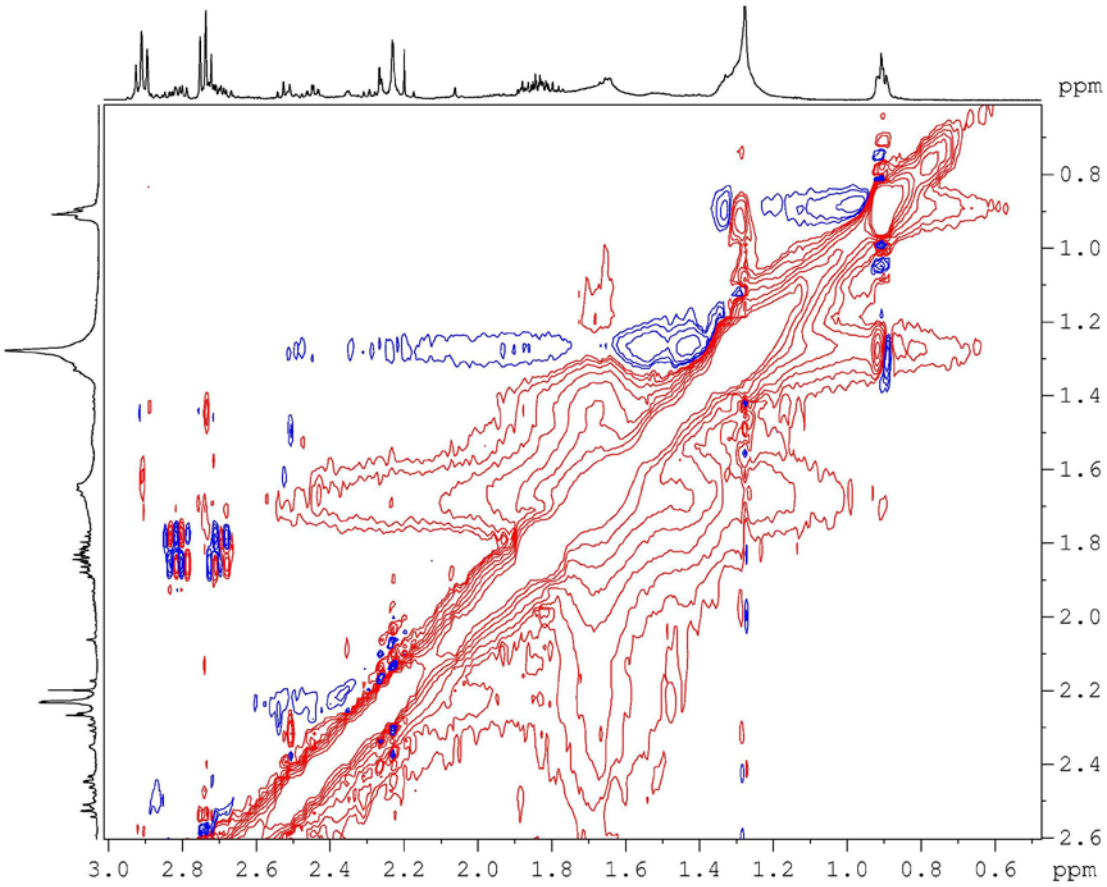

Transferred NOESY NMR shows a negative NOE effect for **N3**. This information points out to a significant interaction of the ligand with the surface of the nanoparticle.

Figure S9. ORTEP drawing of the two non-equivalent molecules of $[PdCl_2(L1)_2]$ (**C1**), showing all non-hydrogen atoms and the atom numbering scheme; 50% probability amplitude displacement ellipsoids are shown.

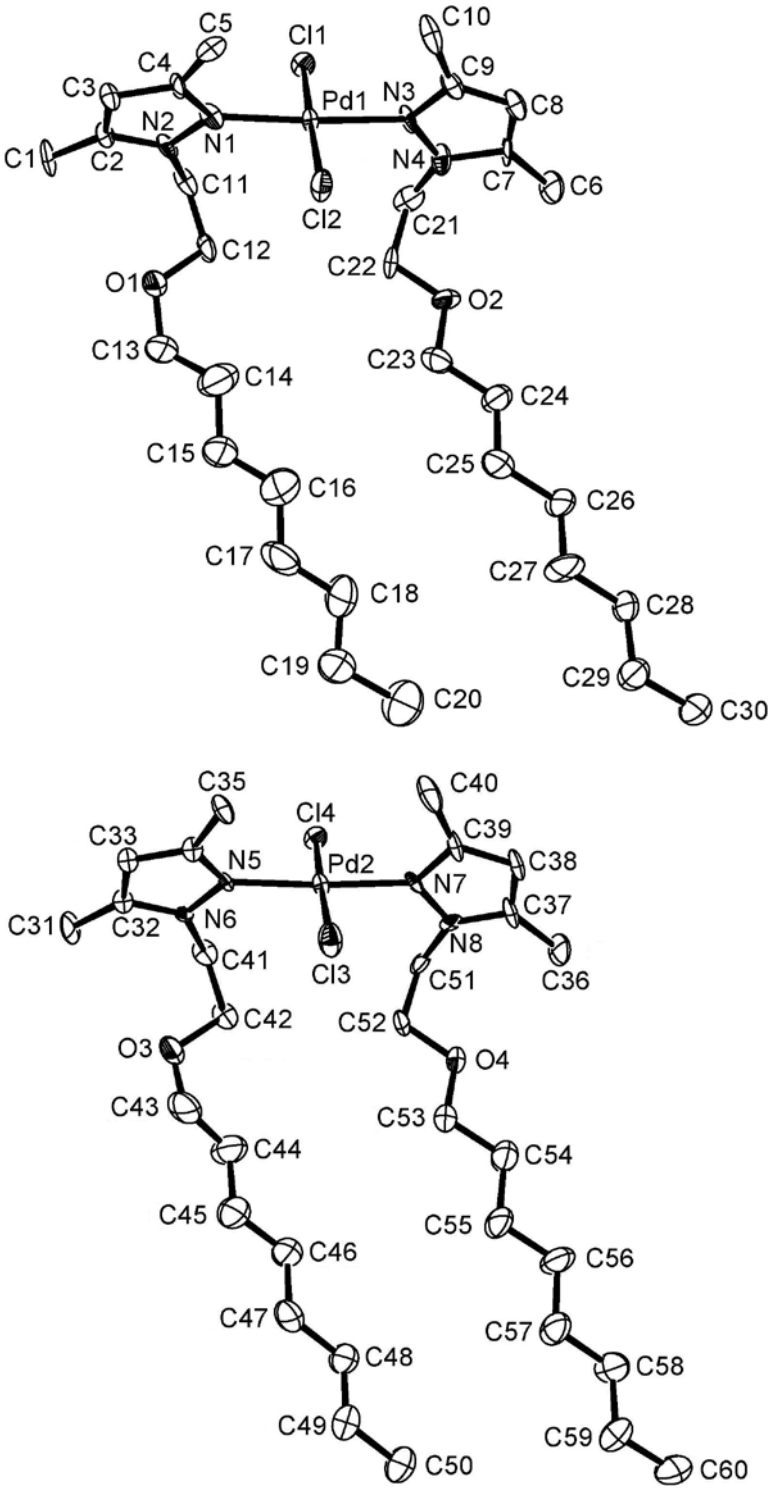

Figure S10. ORTEP drawing of the two non-equivalent molecules of $[PdCl_2(L2)]$ (**C2**), showing all non-hydrogen atoms and the atom numbering scheme; 50% probability amplitude displacement ellipsoids are shown.

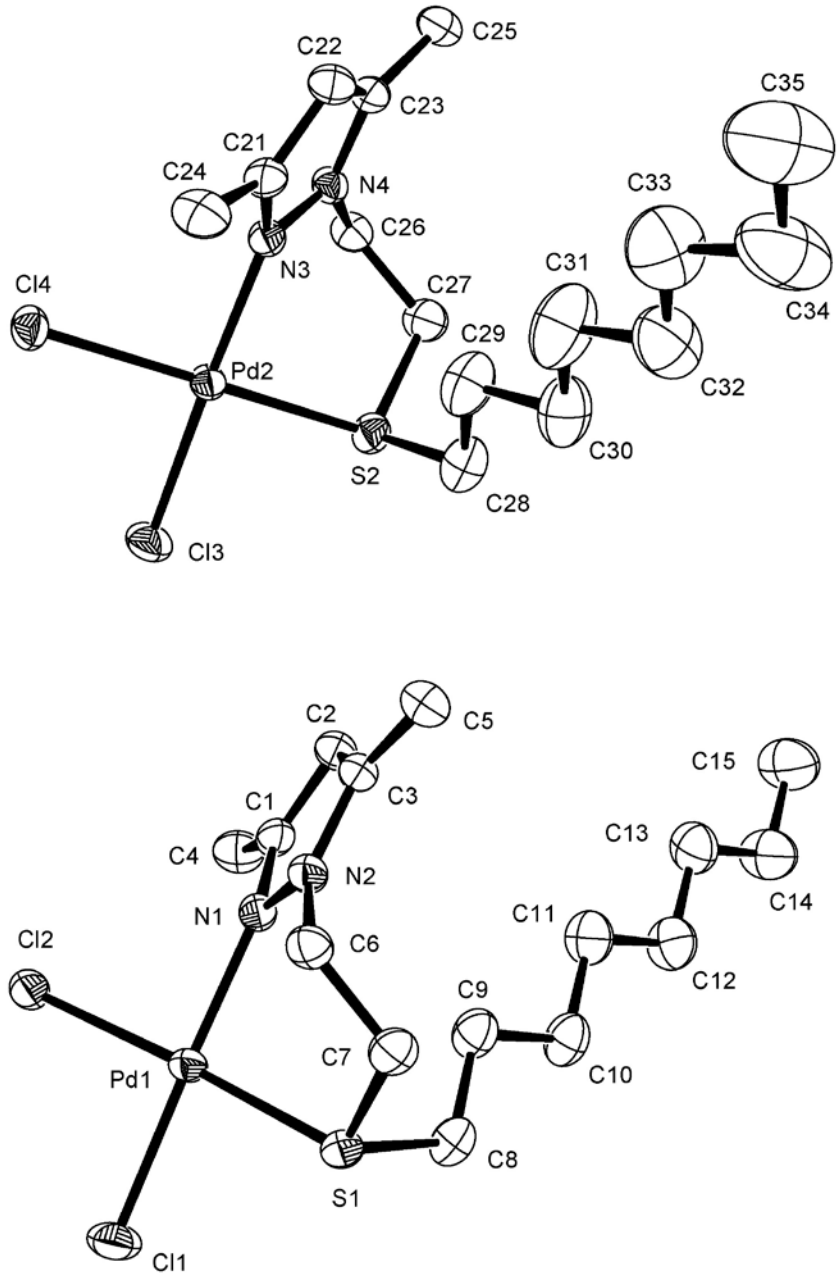

Figure S11. ORTEP drawing of the two non-equivalent molecules of [$PdCl_2$(L3)] (**C3**), showing all non-hydrogen atoms and the atom numbering scheme; 50% probability amplitude displacement ellipsoids are shown.

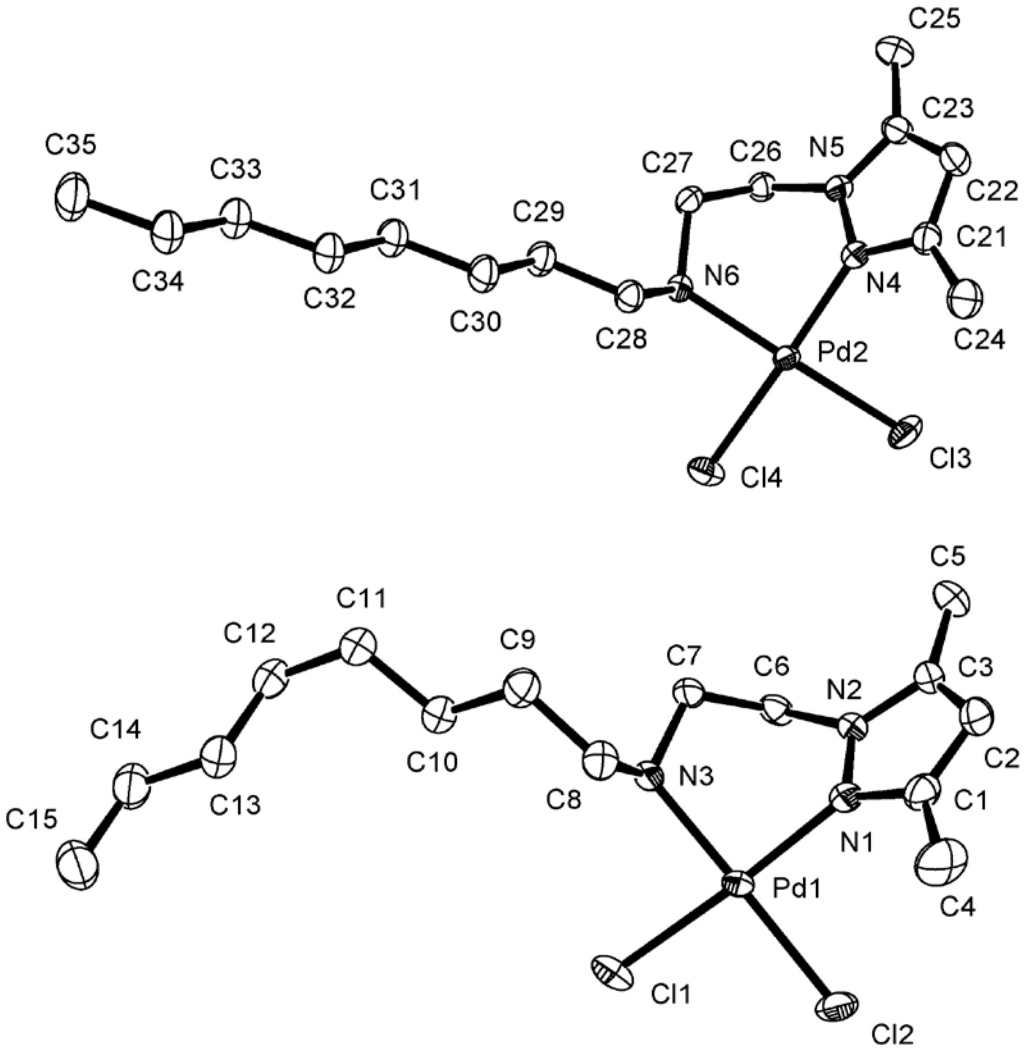

Figure S12. DOSY NMR for the "[Pd(0)(dba) $(L1)_2$]" complex

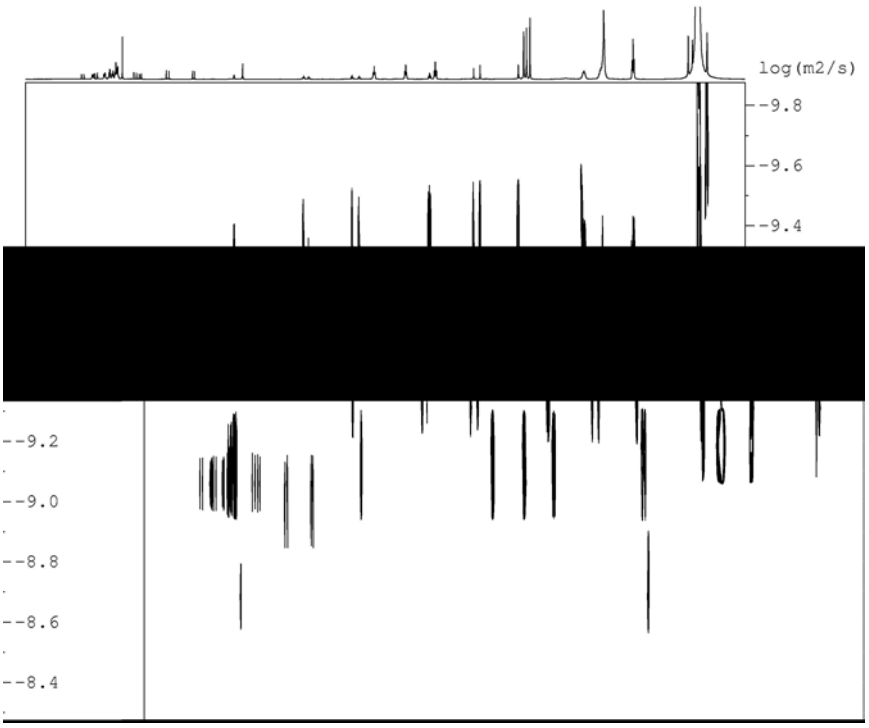

The free ligand **L1** displays a diffusion coefficient of $8.0\pm0.2.10^{-10}$ m^2/s. After reaction with $[Pd_2(dba)_3]$ precursor, a diffusion coefficient of $3.5\pm0.2.10^{-10}$ m^2/s is obtained for the coordination complex. Therefore, the hydrodynamic radius for the Pd(0) complex is about twice that of the free **L1** ligand, suggesting that two **L1** ligands are coordinated to each Pd center.

Figure S13. DOSY NMR spectrum for the "[Pd(0)(dba)(L3)]" complex.

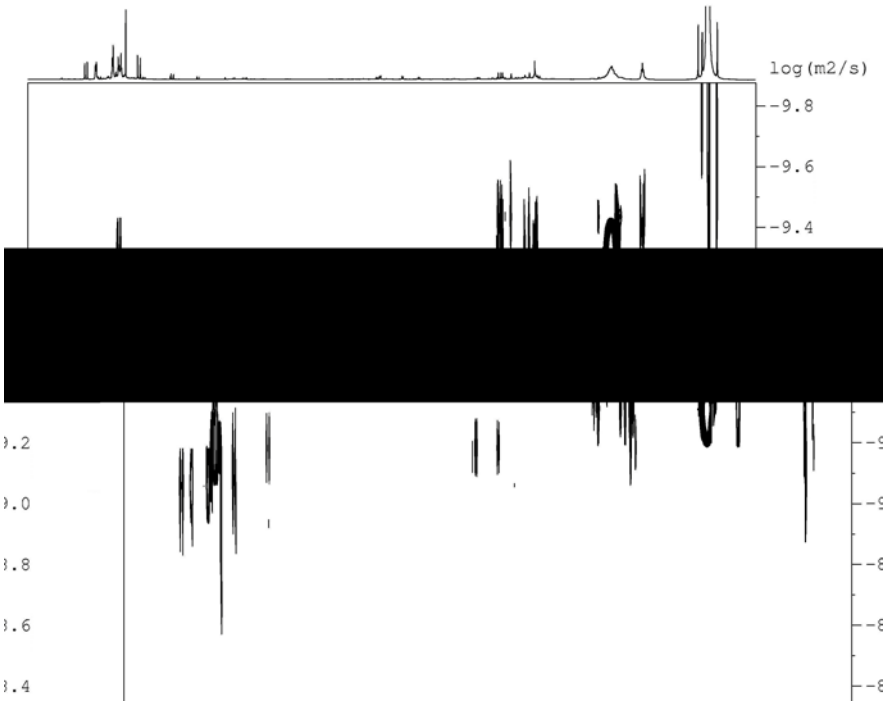

As expected, the **L3** ligand showed the same diffusion coefficient as **L1**. The DOSY NMR spectra of $[Pd_2(dba)_3]$ plus **L3** solutions show at least three different complex species. In two of them, the ligand seems to be coordinated through the azine nitrogen of the pyrazole ring.

NMR Studies of C1-C4

Solution NMR of **C1-C4** complexes was investigated to obtain information about the coordination behavior of **L1-L4** in solution. The ^{1}H NMR spectrum of **C1** at room temperature is similar to that of the free ligand, except that two sets of triplets are observed for each CH_2 of the NCH_2CH_2O moiety. These two sets of triplets arise from two conformers, *syn* and *anti*, (in 41/59 ratio) in a slow dynamic equilibrium. The interconversion of these conformers takes place through a slow rotation of the Pd-N bonds, which is hindered by the methyl substituents of the pyrazole ring and the chloro ligands.

In the ^{1}H NMR spectrum of **C2** at room temperature, again only the signals corresponding to NCH_2CH_2S fragment differ significantly from those of the free ligand **L2**. In **C2**, these methylenic protons appear as two ill-defined broad bands, suggesting that a dynamic equilibrium is taking place in solution. By lowering the temperature to 223 K, each of the two broad bands split into two well-defined sets of signals. The coalescence temperature for this process (283 K) and the separation of the two signals attributed to each CH_2 corresponds to a $\Delta G^{\ddagger}$ value of 53 $kJ \cdot mol^{-1}$. This $\Delta G^{\ddagger}$ value is consistent with a process involving the ring-flipping of the PdNNCCS metallacycle due to the rotation of the Pd-N bond without bond breaking, although this process could also be explained by a mechanism involving the inversion of configuration of the sulfur atom.

The ^{1}H NMR spectrum of **C2** at 223 K is similar to those of **C3** and **C4** at room temperature. This corroborates that the three complexes have ligands **L2-L4** coordinated in a chelating mode. It is also evident that, contrary to **C2**, **C3** and **C4** are not involved in dynamic equilibrium process at room temperature. The latter suggests

that the dynamic equilibrium observed in **C2** should arise from the sulfur inversion, since the Pd-N rotation barrier should be very similar in the three complexes.

This chelating coordination mode of **L2-L4** in **C2-C4** freezes the methylene conformations of the $N_{pz}CH_2CH_2X$ (X = S, N) fragment, making each CH_2 moiety diastereotopic. This led to four groups of signals, each of them associated to a single hydrogen. These signals appear as a doublet of doublets of doublets, arising from a geminal ^2J coupling and two vicinal ^3J coupling constants.